

TESS Timings of 31 Hot Jupiters with Ephemeris Uncertainties

SU-SU SHAN,^{1,2} FAN YANG,^{1,3,2} YOU-JUN LU,^{1,2} XING WEI,³ WEN-WU TIAN,^{1,2} HAI-YAN ZHANG,¹ RUI GUO,⁴ XIAO-HONG CUI,¹
 AI-YUAN YANG,⁵ BO ZHANG,³ AND JI-FENG LIU^{1,2,6}

¹*National Astronomical Observatories, Chinese Academy of Sciences, 20A Datun Road, Chaoyang District, Beijing 100101, China*

²*School of Astronomy and Space Science, University of Chinese Academy of Sciences, Beijing 100049, China*

³*Department of Astronomy, Beijing Normal University, Beijing 100875, People's Republic of China*

⁴*Department of Astronomy, School of Physics and Astronomy, Shanghai Jiao Tong University, 800 Dongchuan Road, Shanghai 200240, China*

⁵*Max Planck Institute for Radio Astronomy, Auf dem Hügel 69, 53121 Bonn, Germany*

⁶*WHU-NAOC Joint Center for Astronomy, Wuhan University, Wuhan, China*

ABSTRACT

A precise transit ephemeris serves as the premise for follow-up exoplanet observations. We compare TESS Objects of Interest (TOI) transit timings of 262 hot Jupiters with the archival ephemeris and find 31 of them having TOI timing offsets, among which WASP-161b shows the most significant offset of -203.7 ± 4.1 minutes. The median value of these offsets is 17.8 minutes, equivalent to 3.6σ . We generate TESS timings in each sector for these 31 hot Jupiters, using a self-generated pipeline. The pipeline performs photometric measurements to TESS images and produces transit timings by fitting the light curves. We refine and update the previous ephemeris, based on these TESS timings (uncertainty ~ 1 minute) and a long timing baseline (~ 10 years). Our refined ephemeris gives the transit timing at a median precision of 0.82 minutes until 2025 and 1.21 minutes until 2030. We regard the timing offsets mainly originating from the underestimated ephemeris uncertainty. All the targets with timing offset larger than 10σ present earlier timings than the prediction, which cannot be due to underestimated ephemeris uncertainty, apsidal precision, or Rømer effect as those effects should be unsigned. For some particular targets, timing offsets are likely due to tidal dissipation. Our sample leads to the detection of period decaying candidates of WASP-161b and XO-3b reported previously.

Keywords: Exoplanet systems (484), Exoplanet astronomy (486), Transit photometry(1709), transit timing variation method (1710)

1. INTRODUCTION

Transit ephemeris is crucial for exoplanet follow-up investigations, e.g., atmosphere analysis (Berta et al. 2012; Deming et al. 2013; Yang et al. 2021) and orbital evolution (Lendl et al. 2014; Dawson & Johnson 2018; Millholland & Laughlin 2018; Yee et al. 2020). The newly commissioned Transiting Exoplanet Survey Satellite (Ricker et al. 2015, TESS) provides precise timings in a long baseline when combined with previous works, which enables us to obtain a better transit ephemeris.

The observed transit timing could deviate from the ephemeris prediction due to either underestimation of ephemeris uncertainties (Mallonn et al. 2019), or physical

processes (Agol & Fabrycky 2018). The TTV could originate from tidal dissipation, orbital precession, Rømer effect, mass loss and multi-planets (Patra et al. 2017; Yee et al. 2020; Turner et al. 2021; Bouma et al. 2020; Ragozzine & Wolf 2009; Lai et al. 2010; Mazeh et al. 2013; Agol & Fabrycky 2018). For hot Jupiters, the interactions of planet companions are usually not massive and close enough to generate significant TTVs (Huang et al. 2016; Dawson & Johnson 2018).

TTV provides direct evidence of tidal dissipation that likely drives hot Jupiter migration (Dawson & Johnson 2018). WASP-12b has been reported to undergo tidal dissipation by observational TTVs (Patra et al. 2017; Yee et al. 2020; Turner et al. 2021). The TTVs are at the level of ~ 5 minutes in a 10-year baseline compared to the ephemeris obtained from a constant period (Yee et al. 2020). Apsidal precession is reported to be the major arguing explanation and seems to be ruled out with more than 10-year observations, including most recent TESS timings (Patra et al. 2017; Yee et al. 2020;

Fan Yang: sailoryf@nao.cas.cn; sailoryf1222@gmail.com

Ji-Feng Liu: jfliu@nao.cas.cn

Turner et al. 2021). The referred works also discuss and exclude the other possible effects, including Rømer effect and mass loss (Ragozzine & Wolf 2009; Lai et al. 2010).

The Rømer effect, i.e. the acceleration towards the line-of-sight probably due to stellar companions, has been reported to dominate the TTV of WASP-4b (Bouma et al. 2020). Using TESS light curves, Bouma et al. (2019) present a period decreasing at $-12.6 \pm 1.2 \text{ ms yr}^{-1}$. Further radial velocity (RV) monitoring indicates the Doppler effect contributes most of the period decreases (Bouma et al. 2020). For another example, WASP-53b and WASP-81b should harbor brown dwarf companions which could cause TTVs $\sim 30\text{s}$, according to the calculation of Triaud et al. (2017).

We compare TESS timings and archival ephemeris predictions¹, and report transit timing offsets of 31 hot Jupiters in this work. The paper is organized as follows. We present the sample selection and data reduction in Section 2. In Section 3, transit timings and offsets compared to the previous ephemeris are shown. The ephemeris refinement is also shown in this section. In Section 4, we discuss the possible physical origin of the timing offsets. We briefly summarize the work in Section 5.

2. SAMPLE SELECTION AND TESS TIMING

The exoplanet sample in this work are hot Jupiters identified from previous work and have access to transit timings from the TESS Objects of Interest (TOI) Catalog (Guerrero et al. 2021). The archival data is extracted from the NASA Exoplanet Archive (Akeson et al. 2013) 10.26133/NEA12 table as of August 2021. The sample selection requires an orbital period of fewer than 10 days, a planet mass larger than $0.5 M_J$, and a planet radius larger than $0.5 R_J$. These criteria leave 421 hot Jupiters. After crossmatched this sample and the TOI catalog, we find out TESS observed and reported new transit timing for 262 hot Jupiters.

2.1. TESS Photometry and TOI Catalog

TESS is launched in 2018, possessing four cameras with a total field of view (FOV) of 24×96 square degrees, equivalent to a pixel resolution of 21 arcseconds (Ricker et al. 2015). The full frame image (FFI) covering FOV is released in a cadence of 30 minutes (as shown in Figure 1) while $\sim 200,000$ targets are recorded with 11×11 pixel cut-off images in a cadence of 2 minutes (known as target pixel file; TPF). The TESS data is available in MAST: [10.17909/t9-yk4w-zc73](https://doi.org/10.17909/t9-yk4w-zc73), [10.17909/t9-nmc8-f686](https://doi.org/10.17909/t9-nmc8-f686).

The TOI catalog is built based on the light curves obtained from TESS image products, including both 2 minute and 30 minute frames (Guerrero et al. 2021). The 2-minute cadence

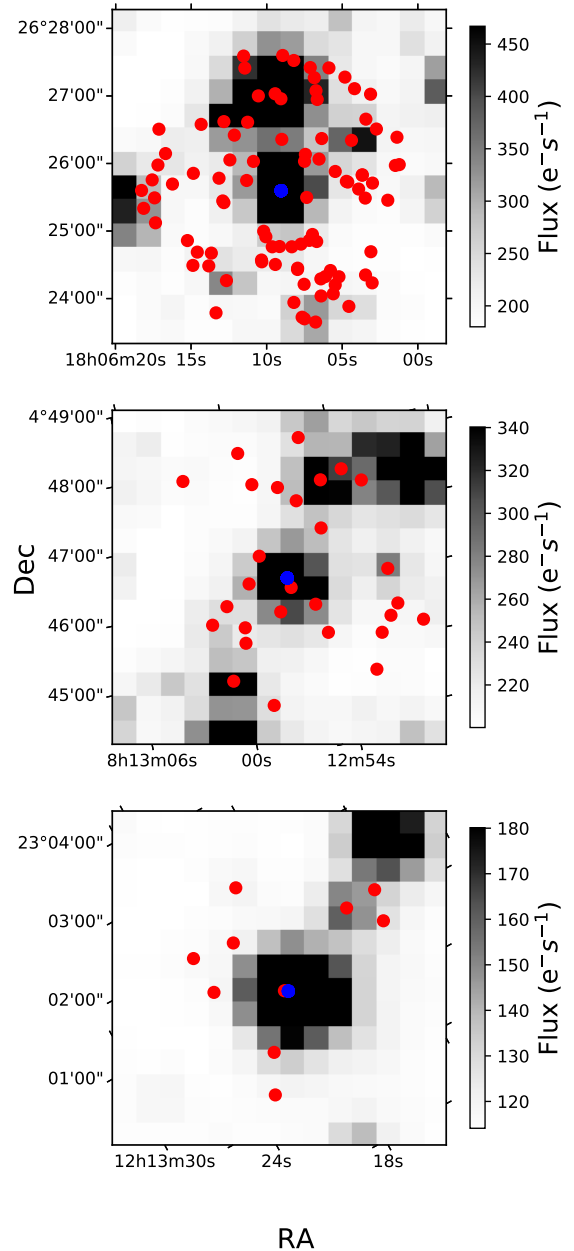


Figure 1. TESS example images of 14×14 pixels. The images correspond to HAT-P-31b, HAT-P-35b, and WASP-56b, from top to bottom. The blue points refer to the planet position in the Gaia catalog (Gaia Collaboration et al. 2018a) while red points present nearby source positions.

¹ Exoplanet Archive: <https://exoplanetarchive.ipac.caltech.edu/index.html>

light curve is generated by the Science Processing Operations Center (SPOC) pipeline and the 30 minute light curves by the Quick Look Pipeline (QLP) (Twicken et al. 2016; Huang et al. 2020). Guerrero et al. (2021) generate an automated pipeline to derive transit parameters and thereby identify planet candidates with the method referred to the Kepler Robovetter (Thompson et al. 2018). More than 2000 planet candidates (continuously updating) are identified in the TOI catalog including both newly discovered and previously known planets.

The timing from the TOI catalog provides a long time baseline when compared with the previous ephemeris. The median timing baseline of the 262 exoplanets is 2368 days, while the median uncertainties of timings from archival data and from the TOI catalog are 0.59 and 0.84 minutes. The median uncertainty of archival periods is 4×10^{-6} days. 159 of 262 hot Jupiters show consistent TESS timings within 1σ when compared to the previous ephemeris predictions. This circumstantially demonstrates the accuracy of TOI timings. We neglect the difference between the Barycentric Julian Date (BJD) and Heliocentric Julian Date (HJD) in this work. The difference is within ± 4 s, beyond the timing precision discussed.

The TOI catalog has been well utilized for exoplanet research, including TTV analysis which uses the data in a similar condition to this work (Pearson 2019; Martins et al. 2020; Howard et al. 2021).

2.2. TESS Transit Timing Acquirement

A precision validation of TOI timing is necessary, for the purpose of the study on timing offsets to the previous ephemeris. A majority of the hot Jupiters (159 of 262) present consistent TOI timings which could be circumstantial evidence. Direct evaluation is performed by independently reducing the data and obtaining the TESS timings. We generate a half-automatic pipeline to obtain and fit the light curve from TESS images (Yang et al. 2022a, 2021).

The pipeline includes two parts, i.e., a photometric pipeline and transit modeling. The photometric pipeline works on TESS image products (as shown in Figure 1) and includes modules: e.g., astrometry checking, aperture photometry, de-blending of the nearby contamination flux, and light curve detrending. The photometric pipeline generates light curves from raw images of both 30-minute cadence (FFI) and 2-minute cadence (TPF). During TESS extended mission, the 30-minute cadence FFI is updated with a 10-minute cadence. The 10-minute FFI is used in our pipeline. Currently, we do not search for the recently released 20-second cadence data.

The photometric data reduction starts at finding if the TPF is available for the source. We would use 2-minute cadence TPF for light curve generation and 30-minute cadence FFI cut-off as a substitution when TPF is not available. The as-

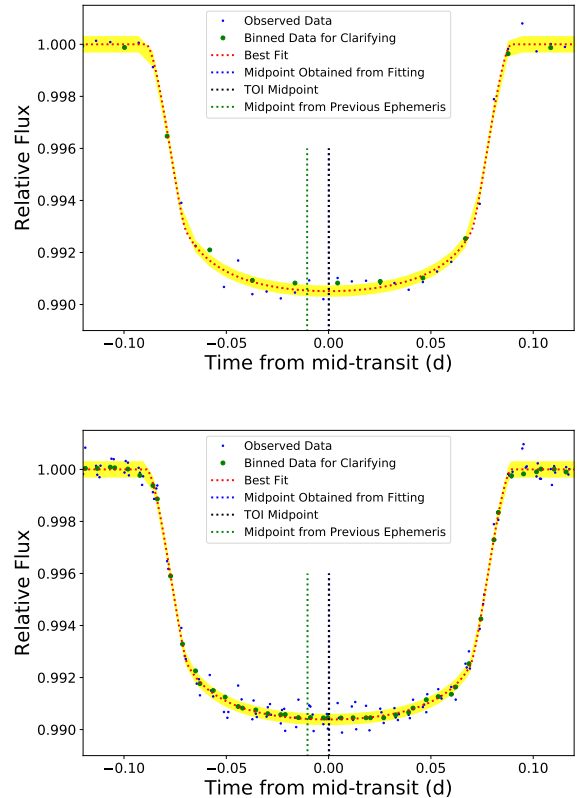


Figure 2. Light curves of KELT-19Ab as an example: single epoch around TOI timing (top panel), folded multiple visits at reference epoch (bottom panel). The blue points present observations (10-minute cadence) while the green points are bins of every three points for clarity. The red line gives the transit model fit with the yellow region indicating 1σ confidence region. The vertical blue line gives the fitted timing; the black vertical line, TOI timing; the green vertical line, previous ephemeris prediction. The timings from single epoch fitting, folded epoch fitting are only 0.14 minutes earlier, 0.20 minutes later than TOI, corresponding to a negligible difference as shown in the image (overlapped blue and black line). The observed TESS timings show an offset of ~ 15 minutes, compared to the previous ephemeris prediction as shown in the vertical green line. The fitting uncertainty is 0.54 minutes for a single epoch, and 0.23 minutes for folded epochs.

trometry would then be checked and corrected if there was any pointing jitter (Yang et al. 2022a; Yang et al. 2021). The astrometry check is based on the comparison between the nominal position reported by Gaia (Gaia Collaboration et al. 2018b) and the target center in the TESS image. Circular aperture photometry is performed with a radius of 63 arcsecs. The background is estimated as the median value of the lowest fifth percentile of pixel fluxes in the vicinity of the target. The photometry error is the quadratic sum of the Poisson error and the standard deviation of the background.

The flux contamination from nearby sources is modeled and removed using the flux profile as a function to the given

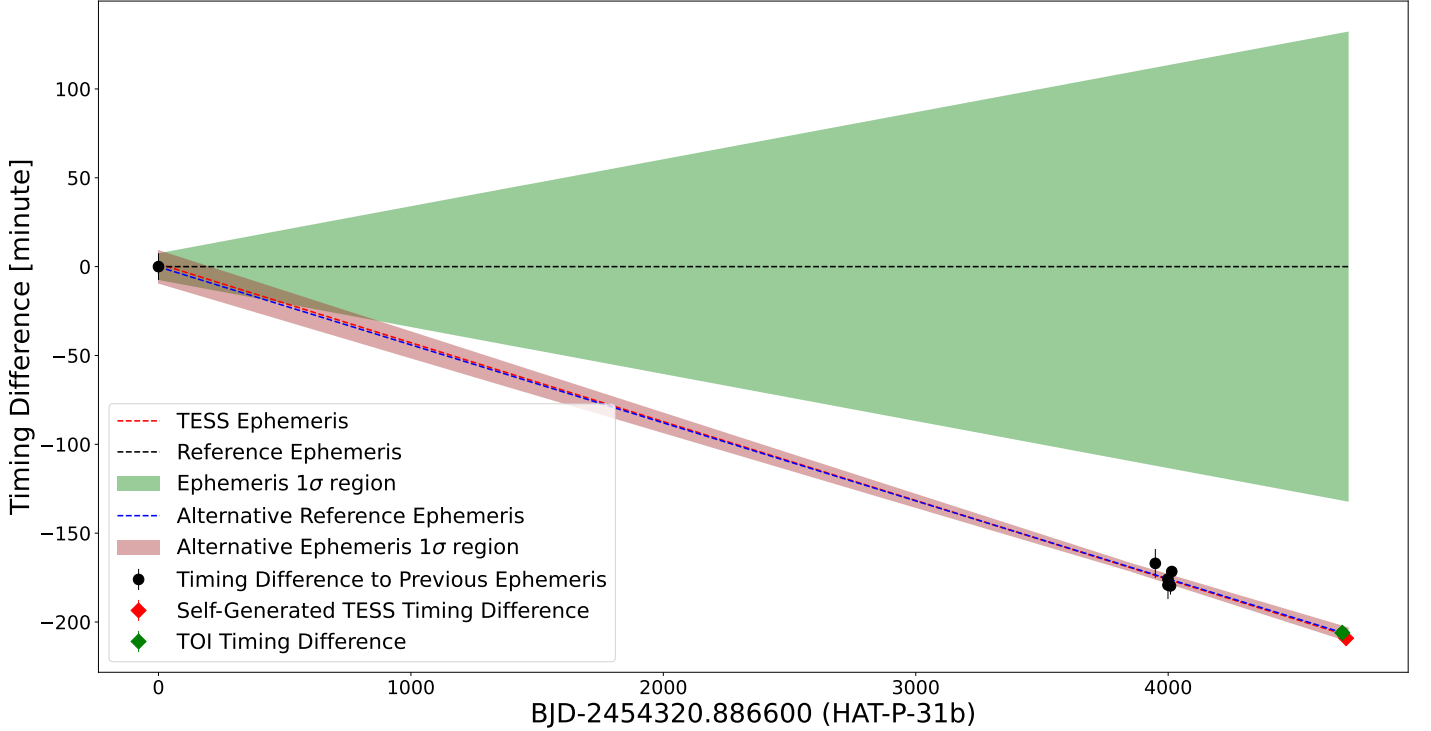


Figure 3. The timing difference of HAT-P-31b. The timing difference is the observed mid-transit times minus the ephemeris predictions. The red point refers to TESS timing difference; black points refer to timing differences of other observations from literature paper (Kipping et al. 2011; Mallonn et al. 2019); the black dashed line is reference ephemeris; blue line alternative reference ephemeris; the red line is the refined ephemeris derived by combining TESS observation; the green region is 1σ significant region of reference ephemeris; the brown region is 1σ significant region of alternative reference ephemeris. We note that our refined ephemeris overlaps the alternative ephemeris, indicating the consistency of the two ephemerides.

center (Yang et al. 2022a). The detrending for long-term structure removing is performed by modeling the light curve of 0.6 days centering at the transit mid-point after masking the planetary transit. We use a linear function for modeling the long-term structure. We have tested with high order polynomial functions (up to 10 orders) as well as a cubic spline function which gives negligible differences for five validation targets in this work and the exoplanets investigated in previous work (Yang et al. 2022a; Yang et al. 2021; Yang et al. 2021).

The detrended light curve is performed with a stellar activity check from archival data and TESS photometry to avoid possible timing bias. The strong stellar activity would be taken into consideration. We note that the starspot perturbation is more significant to brightness than to the shape of the light curve unless the transit comes across the starspot (Makarov et al. 2009; Agol et al. 2010). Among the comparison sample in this work, we do not find any significant transit across starspot. Empirically, a sun-like star would hold a variability at a level of ~ 10 ppm on planet transit timescale (Jenkins 2002). In addition, the bias of timing estimation caused by starspot would be weakened by detrending process.

More details and evaluations of the pipeline are referred to in previous work (Yang et al. 2022a, 2021). From the tests and applications so far, the derived transit parameters are within 1σ when we apply the same fitting to TPF light curves.

We derive timings of 31 hot Jupiters using our self-generated pipeline. And we check if the timing obtained from our pipeline is consistent with TOI timing and find the difference is commonly within 2 minutes. Comparison details are present in Section 3.

Applying Markov Chain Monte-Carlo (MCMC) (Patil et al. 2010; Czesla et al. 2019), the light curve is fitted with a planet transit model (Mandel & Agol 2002; Eastman et al. 2013). The choice of ‘circular orbit’ or ‘Keplerian orbit’ is consistent with the archival reference work. We briefly describe the transit modeling here with more details available in (Yang et al. 2022a, 2021).

For ‘circular orbit’, the free parameters during our fitting are transit mid-point (T_0), the radius ratio of planet to star (R_p/R_*), the semi-major axis (a/R_*), and the limb darkening parameters. For ‘Keplerian orbit’, the model has extra free parameters (during our fitting) of the longitude of the ascending node, the orbital eccentricity (e), the ascending node,

the periapsis passage time, and the periapsis argument (ω). The fitting model as well as parameterization are taken from (Eastman et al. 2013), e.g., formats of e and ω are $\sqrt{e}\sin\omega$ and $\sqrt{e}\cos\omega$.

The MCMC fitting runs 50,000 steps after the first 50,000 steps as initialization. All the priors are uniform, except for the limb darkening which applies Gaussian prior interpreted in limb darkening table (Claret 2018). We apply quadratic law (Sing 2010; Kipping 2013) for parameterizing limb darkening in this work. Specifically, the format is standard parameterization of u_1, u_2 . The uncertainty of the light curve applied for obtaining MCMC final result is the standard deviation of the light curve residual from an initial fitting. We do not apply a time-dependent term nor a jitter term for the uncertainty given that no significant evidence of time-dependent and jitter structures has been found during the previous TESS research experiences (Yang et al. 2022a, 2021; Yang et al. 2021; Yang & Wei 2022). We note that extra free parameters during fitting may reduce the fitting χ^2 which might be considered in future applications.

We apply the transit model to both the light curve of a single epoch and the light curve folded from one TESS sector (examples as shown in Figure 2). The folding is based on the archival ephemeris and we evaluate the fitting parameter bias if folding an inappropriate period (using the same method as in Yang et al. 2021). For TESS one sector, the timing bias is ~ 4 minutes if the period is biased at 0.0004 days. Such large period bias would cause significant TESS timing offsets when compared to ephemeris prediction and thereby are flagged. The fold-and-check method has been well utilized in period searching researches (Schwarzenberg-Czerny 1989; Yang et al. 2020; Yang et al. 2021). In this work, we utilize and present the final timings obtained from folded light curves in one TESS sector. TOI timings are used for sample selection.

The oversampling technique is applied to mitigate influences caused by the sampling rate of TESS 30 minute data. (Kipping 2010) reports transit parameter bias caused by under-sampling and proposes the oversampling technique using a numerical solution to Kepler's equation. In previous work, we discuss the sampling influence on inclination and transit depth with and without oversampling technique (Yang et al. 2022a). In this work, we check if timing precision could improve by oversampling technique. The median timing uncertainty is ~ 4 minutes for modeling to 30-minute cadence light curve without oversampling. The timing uncertainty is ~ 1 minute for the 2-minute cadence light curve. Applying oversampling routine from (Kreidberg 2015), we resample the 30-minute light curve to the cadences of 1-minute, 2-minute, and 10 minutes. The timing uncertainties obtained from fitting the resampled light curves are the same as the result when not applying the oversampling technique. We also

test the oversampling to the 2-minute cadence light curve obtained from TPF. The resampling rate is set to be 0.5 and 1 minute. The test also yields a negligible timing difference. We note that the oversampling is particularly effective in estimating inclination as described in (Yang et al. 2022a).

An extra timing uncertainty would be induced to be up to a few 0.1 minutes for the 30-minute light curve. The FFI cut-off we use sets the time stamp as the same as the time of the FFI center. The timing difference during BJD to JD switching can be as large as 0.5 minutes for sources on CCD center and corner that TESS CCD is at 12 degrees \times 12 degrees size. This extra uncertainty is negligible considering the uncertainty of 4 minutes for timings obtained from the FFI cut-off. 2-minute light curves do not suffer such an issue that the time correction has been performed to TPF.

The median timing offset between our results and TOI timings is 1.43 minutes among test sample. The median TOI timing uncertainty is 0.83 minutes. We conclude that it is reasonable to use TOI timings. And the TOI timing offset to the previous ephemeris is regarded as significant if the offset is larger than 4 minutes which is ~ 3 times the median difference. We also require the timing offset to be larger than 1 combined σ which is the square root of the quadratic sum of archival ephemeris uncertainty and TESS timing uncertainty. These criteria lead to a final sample of 31 hot Jupiters.

3. HOT JUPITERS WITH TESS TIMING OFFSETS

We obtain a sample of 31 targets with TOI timing offsets compared to the previous ephemeris prediction. An example is shown in Figure 3 with the whole sample as shown in Figure A1. The parameters are present in Table 1, including planet ID, TESS time minus the predicted time from the previous ephemeris (ΔT_C), transit midpoint T_C , orbital period P , reduced chi-squared statistic (χ^2_{red}) of linear period fitting, category flag, parameter reference. We take TOI timings as TESS timings when calculating ΔT_C and replace them with self-generated timings for WASP-173Ab, TOI-1333b, TOI-628b, KELT-21b, KELT-24b, and WASP-187b.

In our sample, the median ΔT_C is 17.8 minutes while the median combined uncertainty is 4.9 minutes. Therefore the signal-to-noise ratio (SNR) is 3.6. Among 31 Jupiters, WASP-161b presents the earliest offset timing of -203.7 ± 4.1 minutes. WASP-17b gives the latest offset timing of 70.8 ± 11.7 minutes. The timing uncertainty is derived as the quadratic sum of uncertainties of previous ephemeris and TESS timing.

We classify the sources into three categories, according to the potential properties implied by the timings. Type I target refers to a source of which timings are modeled with a linear function. The timing inconsistency could be either due to systematic error underestimation or some physical process. The linear function indicates a model with a constant deriva-

tive, referring to a constant period. Type II refers to the targets of which the timing differences can not be modeled by a linear function but by a quadratic function. The quadratic function can be due to abnormal points or physical processes which lead to a constant period derivative. We identify the targets as type III if the timings can not be fitted with any linear or quadratic functions. The possible physical origin of the timing offsets is discussed in Section 4.

Specifically, we present reduced chi-squared (χ^2_{red}) statistic for type I targets if the data set number is larger than 2 (as shown in Table 1). We note that the limited amount

of data sets induces large uncertainty when calculating χ^2_{red} (see details in [Andrae et al. 2010](#)). The Bayesian Information Criterion (BIC, details in [Kass & Raftery 1995](#)) difference for XO-3b is larger than 383, preferring a quadratic function to a linear fit ([Yang & Wei 2022](#)). We note that some hot Jupiters classified as type I may be better fitted with a quadratic function (e.g., WASP-161; [Yang & Chary 2022](#)), though the significance is not as high as XO-3b. These tentative signals need careful following up investigation and are not highlighted in this work.

Table 1. Exoplanet parameters. ‘1’ in column ‘Planet ID’ indicates to the reference ephemeris in Figure 3 and [A1](#), while ‘2’ presents the alternative ephemeris. The TESS timings derived by our pipeline are flagged as this work. The table is sorted by the significance of ΔT_C . Sources with earlier TESS timing are listed before the targets with later TESS timings.

Planet ID	ΔT_C minutes	T_c BJD	P days	χ^2_{red}	Category flags	Reference
WASP-161b 1	-203.7 ± 4.1	2458492.286050 ± 0.00265	5.405366 ± 0.0000039	2.0419	I	This work; Yang & Chary (2022)
		2459249.035676 ± 0.000594				TOI timing
		2457416.5289 ± 0.0011	5.4060425 ± 0.0000048			Barkaoui et al. (2019)
XO-3b 1 2	-17.8 ± 1.2	2458819.06428 ± 0.00035			II	This work; Yang & Wei (2022)
		2458819.064098 ± 0.000279				TOI Timing
		2455292.43266 ± 0.00015	3.19153285 ± 0.0000058			Wong et al. (2014)
		2454449.86816 ± 0.00023	3.1915239 ± 0.0000068			Winn et al. (2008)
		2456419.04365 ± 0.00026	3.19153247 ± 0.0000055			Wong et al. (2014)
KELT-18b 1 2	-26.8 ± 2.3	2458734.280341 ± 0.000335	2.871698 ± 0.0000004	2.7489	I	This work
		2458748.637347 ± 0.000331				
		2458906.582255 ± 0.000325				
		2458932.425443 ± 0.000353				
		2459624.505991 ± 0.000214				
		2459684.811712 ± 0.000239				
		2458714.181140 ± 0.000380				TOI timing
1		2457542.52504 ± 0.00039	2.8717518 ± 0.0000028			McLeod et al. (2017)
		2457542.52463 ± 0.00057	2.8716992 ± 0.0000013			Maciejewski (2020)
WASP-54b 1	-55.9 ± 8.6	2458949.705160 ± 0.001171	3.693599 ± 0.0000006	0.8468	I	This work
		2459573.923274 ± 0.000538				
		2459669.955842 ± 0.000641				
		2458931.236409 ± 0.000435				
		2455518.35087 ± 0.00053	3.6936411 ± 0.0000059			Bonomo et al. (2017)
K2-237b 1	-15.5 ± 3.9	2458642.067579 ± 0.001163	2.180535 ± 0.0000006	7.8139	I	This work
		2459387.806193 ± 0.000636				
		2458626.800781 ± 0.000869				
		2457656.4633789 ± 0.0000048	2.1805577 ± 0.0000057			TOI timing Smith et al. (2019)
WASP-76b 1	-11.9 ± 2.9	2459133.976069 ± 0.000147	1.809881 ± 0.0000002	1.8398	I	This work
		2459472.424209 ± 0.000121				
		2459485.093248 ± 0.000136				
		2459117.687201 ± 0.000119				
		2456107.85507 ± 0.00034	1.809886 ± 0.000001			TOI timing West et al. (2016)
WASP-95b		2458328.690567 ± 0.000287	2.184667 ± 0.0000002	1.1205	I	This work

Continued on next page

Table 1 – *Continued from previous page*

Planet ID	ΔT_C minutes	T_c BJD	P days	χ^2_{red}	Category flags	Reference
1	-10.7±2.9	2459075.846388±0.000132 2459084.585010±0.000110 2456338.458510±0.000240	2.184673±0.0000014			TOI timing Hellier et al. (2014)
WASP-101b	-17.3±5.2	2458481.061101±0.000185 2459216.130731±0.000145 2459223.302264±0.000132 2456164.6934±0.0002	3.585708±0.0000003 3.585722±0.000004	4.4892 2	I	This work TOI timing Hellier et al. (2014)
WASP-35b	-9.5±3.5	2458459.092397±0.000244 2459179.930001±0.000126 2459176.768453±0.000197 2455531.479070±0.000150	3.161569±0.0000002 3.161575±0.0000020	0.2758	I	This work TOI timing Enoch et al. (2011)
TOI-163b	-57.2±22.0	2458350.038867±0.000908 2458371.194185±0.001123 2458392.345356±0.001497 2458421.969304±0.000841 2458451.585295±0.001530 2458481.204317±0.000995 2458557.363318±0.001196 2458574.287291±0.000781 2458612.367794±0.000928 2458629.292355±0.001017 2458671.603439±0.000874 2459039.709508±0.000636 2459073.556184±0.000635 2459069.328010±0.000735 2459098.946501±0.000611 2459132.796272±0.000621 2459175.105352±0.000618 2459204.723621±0.000557 2459234.341314±0.000575 2459263.960120±0.000622 2459331.657993±0.000505 2459348.581531±0.000414 2459373.968750±0.000331 2459310.502979±0.000817 2458328.87970±0.00063	4.231119±0.0000016 4.231306±0.000063	3.2752	I	This work TOI timing Kossakowski et al. (2019)
KELT-14b	-10.7±5.2	2458493.272296±0.000185 2459202.944408±0.000109 2459235.648287±0.000969 2459235.435128±0.000110 2459252.535529±0.000108 2457091.028632±0.000470 2456665.224010±0.000210	1.710054±0.0000001 1.710059±0.0000025 1.710057±0.0000032	4.9021	I	This work TOI timing Rodriguez et al. (2016) Turner et al. (2016b)
KELT-7b		2458816.518431±0.000430 2459492.005468±0.000231 2459519.352936±0.000238	2.734765±0.0000002	3.3771	I	This work

Continued on next page

Table 1 – *Continued from previous page*

Planet ID	ΔT_C minutes	T_c BJD	P days	χ^2_{red}	Category flags	Reference
1	-12.4±5.4	2459533.027055±0.000234	2.734775±0.0000039			TOI timing Bieryla et al. (2015)
		2458819.253410±0.000240				
		2456355.229809±0.000198				
HAT-P-31b	-206.0±131.6	2459025.840900±0.001368	5.005269±0.0000056	0.9519	I	This work TOI timing
		2459010.826736±0.001149	5.005425±0.000092			Kipping et al. (2011) Mallonn et al. (2019)
		2454320.8866±0.0052				
		2458169.9410±0.0017	5.0052724±0.0000063			
KELT-1b	-67.4±53.9	2458765.534321±0.000717	1.217494±0.0000003	7.4954	I	This work TOI timing
		2458765.533813±0.000299	1.217514±0.000015			Siverd et al. (2012) Baluev et al. (2015)
		2455914.1628±0.0023				
		2456093.13464±0.00019	1.21749448±0.0000080			
KELT-21b	-0.59±2.5	2458690.462229±0.000704	3.612769±0.0000008	3.4411	I	This work
		2458719.364524±0.000912	3.612765±0.0000030			TOI timing Johnson et al. (2018)
		2459420.242127±0.000267				
		2458686.841940±0.000580				
HAT-P-69b	9.7±1.5	2459247.345980±0.000274	4.786949±0.0000018		III	This work
		2458510.155715±0.000546				TOI timing
		2459242.559429±0.000245				Zhou et al. (2019)
		2458495.788610±0.000720				
WASP-17b	70.8±11.7	2458638.332379±0.000340	3.735485±0.0000003	5.5856	I	This work
		2459340.602164±0.000403	3.735442±0.0000072 3.7354380±0.0000068 3.7354845±0.0000019 3.735438			TOI timing Anderson et al. (2010) Anderson et al. (2011) Southworth et al. (2012) Sedaghati et al. (2016)
		2458627.126221±0.000584				
		2454559.181020±0.000280				
		2454577.85806±0.00027				
		2454592.80154±0.00050				
		2457192.69798±0.00028				
WASP-178b	12.9±3.1	2458609.523699±0.000421	3.344839±0.0000007	3.4716	I	This work
		2459352.077016±0.000181	3.344829±0.0000012 3.344841±0.0000033			TOI timing TOI timing Hellier et al. (2019) Rodríguez Martínez et al. (2020)
		2458602.836430±0.001860				
		2459358.7671460±0.0003877				
		2456927.068390±0.000470				
		2458321.867240±0.000380				
WASP-33b	22.4±6.9	2458814.59179±0.000193	1.219871±0.0000001	4.8662	I	This work
		2458791.414307±0.000169	1.219867±0.0000012 1.219868±0.0000011			TOI timing Collier Cameron et al. (2010) von Essen et al. (2014)
		2454163.223730±0.000260				
		2455507.522200±0.000300				
KELT-23Ab		2458701.953602±0.000164			III	This work
		2458719.996122±0.000187				
		2458758.335680±0.000196				
		2458765.102458±0.000197				
		2458895.908656±0.000170				
		2458934.248842±0.000181				
		2459443.943092±0.000132				
		2459599.557734±0.000131				
		2459613.090493±0.000169				

Continued on next page

Table 1 – *Continued from previous page*

Planet ID	ΔT_C minutes	T_c BJD	P days	χ^2_{red}	Category flags	Reference
1 2	23.8±7.7	2459651.430016±0.000135				TOI timing Johns et al. (2019) Maciejewski (2020)
		2459669.472623±0.000142				
		2459793.513154±0.000138				
		2458683.911214±0.000056	2.255251±0.0000110			
		2458140.379200±0.002700	2.255288±0.0000007			
		2458140.386980±0.000200				
HAT-P-6b 1	26.3±9.2	2458759.452299±0.000648	3.852999±0.0000004	7.5980	I	This work
		2458774.864299±0.000681				TOI timing Noyes et al. (2008)
		2458740.188710±0.000360	3.852985±0.0000050			
		2454035.675750±0.000280				
KELT-19Ab 1	15.2±5.9	2459222.7898588±0.00020	4.611736±0.0000009	4.1958	I	This work
		2458507.971344±0.0002751				TOI timing Siverd et al. (2018a)
		2459222.789720±0.000183	4.611709±0.0000088			
		2457281.249537±0.000361				
WASP-94Ab 1	10.2±4.0	2458352.000206±0.000642	3.950201±0.0000006	0.5179	I	This work
		2459039.335697±0.000323				TOI timing Bonomo et al. (2017)
		2459039.335846±0.000386	3.950191±0.0000037			
		2456416.402150±0.000260				
WASP-58b 1 2	37.4±13.5	2458695.984265±0.000376	5.017215±0.0000005	2.7651	I	This work
		2458706.018411±0.000428				TOI timing Hébrard et al. (2013) Mallonn et al. (2019)
		2458991.998531±0.000371				
		2459017.084690±0.000379				
		2459413.444427±0.000157				
		2459734.547119±0.000164				
WASP-99b 1	61.6±31.2	2459764.650223±0.000159				TOI timing Bonomo et al. (2017)
		2458986.981902±0.000409				
		2455183.933500±0.001000	5.017180±0.0000110			
		2457261.059700±0.000620	5.017213±0.0000026			
TOI-1333b 1	2.67±1.4 -5.7±1.5	2458715.1230±0.0010	4.720171±0.0000204	0.0318	I	This work
		2458752.884599±0.000828				TOI timing Rodriguez et al. (2021)
		2458715.117140±0.000550				
		2458913.370330±0.000450	4.720219±0.0000110			
WASP-78b 1 2	18.8±11.1	2458446.902114±0.000472	2.175185±0.0000003	3.9626	I	This work
		2459162.537455±0.000227				TOI timing Bonomo et al. (2017) Brown et al. (2017)
		2459192.991391±0.000379				
		2459175.589610±0.000863				
WASP-173Ab 1	1.2±0.9 -30.4±1.1	2455882.359640±0.000530	2.175176±0.0000047			TOI timing Hellier et al. (2019)
		2456139.030300±0.000500	2.175173±0.0000030			
		2457288.8585±0.0002	1.38665318±0.0000027			

Continued on next page

Table 1 – *Continued from previous page*

Planet ID	ΔT_C minutes	T_c BJD	P days	χ^2_{red}	Category flags	Reference
2		2458105.59824±0.00090	1.3866529±0.0000027			Labadie-Bartz et al. (2019)
TOI-628b	3.8±3.4	2458469.232700±0.002220	3.409512±0.0000335		I	This work
	7.4±1.2	2458469.235200±0.000430				TOI timing
1		2458629.479720±0.000390	3.409568±0.0000070			Rodriguez et al. (2021)
KELT-24b	1.0±0.9	2458695.919325±0.000633 2458868.015428±0.000148 2458895.773212±0.000162 2459412.061344±0.000102 2459423.164772±0.000217 2459606.363810±0.000204 2459617.467116±0.000223 7.9±0.9 2458684.821890±0.000320	5.551490±0.0000011	1.7072	I	This work
1		2458540.477590±0.000360	5.551493±0.0000081			TOI timing
2		2458268.454590±0.000870	5.551492±0.0000086			Rodriguez et al. (2019) Maciejewski (2020)
WASP-187b	7.3±8.7 34.5±8.7	2458785.428921±0.001771 2458764.856300±0.002600 1	5.147885±0.0000027 2455197.352900±0.002000	5.147878±0.0000050	I	This work This work Schanche et al. (2020)

We manually verify the TOI timings of 31 hot Jupiters among which WASP-173Ab, TOI-1333b, and TOI-628b need timing re-calibration. We check the TESS raw data (2-minute cadence) of WASP-173Ab and find an abnormal data point around a transit at 2468356.564637 (BJD). The abnormal data biases the modeling if not clipped when performing an automatic pipeline. The points should be clipped if excess 10σ to the residual of successful transit fitting. We refit the TESS light curve with abnormal data clipped. The timing is 2458355.195662±0.00047 (BJD) when we fit one transit visit and 2458355.195907±0.0001 (BJD) when fitting visits folded through the whole sector. These two results are consistent within 0.35 minutes and are different from TOI timing at 29 minutes. The refitted TESS timing is consistent with the previous ephemeris (as shown in Figure 4).

TOI-1333b timing derived by refitting TESS light curve is 2458715.1230±0.0010 (BJD) which is 8.4 minutes later than TOI derived timing (as shown in Figure 4). The TESS 30 minute data (available for the TOI-1333b) has some abnormal points around transits which would bias the timings if not applying the sigma clipping process. Removing the abnormal data points, we refit the light curve for the timing. The timings derived from single transit and combined transits have a difference of 1.8 minutes (within 0.3 combined σ). The timing is close ($\sim 1\sigma$) to the prediction of previous ephemeris (Figure 4).

We derive a combined timing of 1469.23270±0.00222 (BJD) for TOI-628b while a single transit visit obtains a midpoint at 1469.2332±0.0074 (BJD). The value is $\sim 1\sigma$

earlier than TOI timing and is consistent with the previous ephemeris.

Comparing with our generated TESS timings, TOI timings of KELT-21b, KELT-24b, and WASP-187b present differences of 10, 8, and 35 minutes, respectively. We note that TOI timings are highly reliable given that only 5 sources among 262 TOI hot Jupiters are found with possible issues, referring to a possibility of less than 2%.

3.1. Ephemeris Refinement

We refine the ephemeris of type I targets in our sample. We do not apply any ephemeris refinements to type II and III sources. The new ephemeris consists of TESS timings and a refined period (as shown in Table 1). The period is obtained from a linear fit of TESS timings and timings taken from archival papers (as listed in Table 2) as well as Exoplanet Archive ([Akeson et al. 2013](#)). The refinement has a median precision of 0.82 minutes until 2025 and 1.21 minutes until 2030. The largest uncertainties are 34 minutes in 2025 and 61 minutes in 2030, coming from TOI-628b, due to the shortest baseline. Other than TOI-628b and TOI-1333b, all the refined timing uncertainties are within 5 minutes.

The ephemeris precision depends on the length of the time baseline and transit timing precision. The timing uncertainties could be underestimated due to the techniques in light curve generation and high dimension model fitting ([Yang et al. 2022a, 2021](#)). Combined timing derived from multi-visits based on a constant period assumption might be biased if the folding period is not precise, especially when the light curves partially cover the transits. Correcting the timing bi-

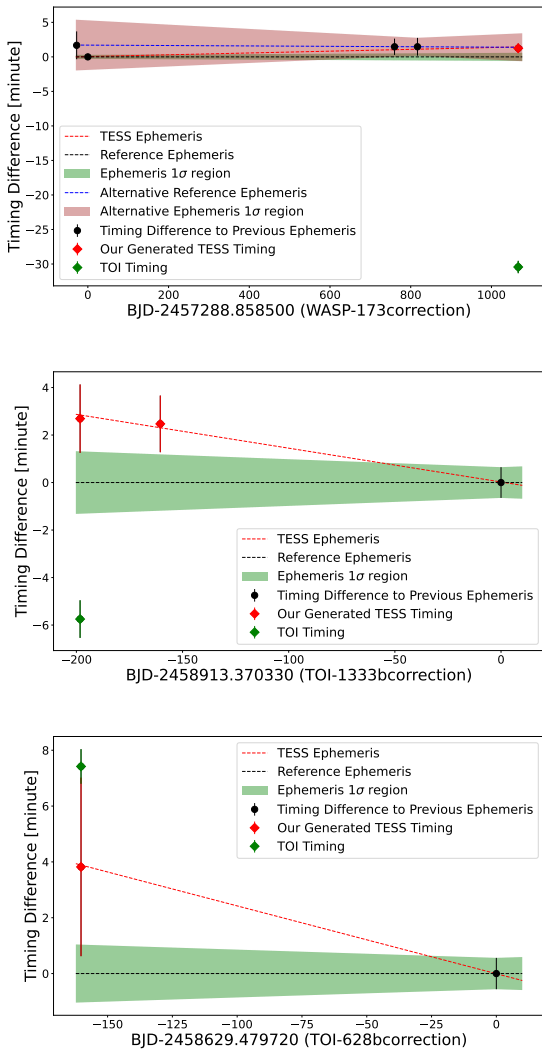


Figure 4. The timing differences with corrected timings for WASP-173Ab, TOI-1333b, TOI-628b. The symbols are similar to Figure 3. The green diamond indicates TOI timing, the red diamond gives the timing generated from TESS raw images.

ases in archival papers (if present) is beyond the scope of this work.

The period could be updated when more observations are available (Mallonn et al. 2019; Edwards et al. 2021a; Wang et al. 2021). The periods from the previous works are significantly different from the periods derived in our refinement. We note that these period differences might origin from physical processes which make the refinement inappropriate (as discussed in Section 4).

4. DISCUSSION: POSSIBLE PHYSICAL ORIGIN

Some targets in our sample present very significant period differences when compared to former results. It might not be a good hypothesis to regard all the differences originat-

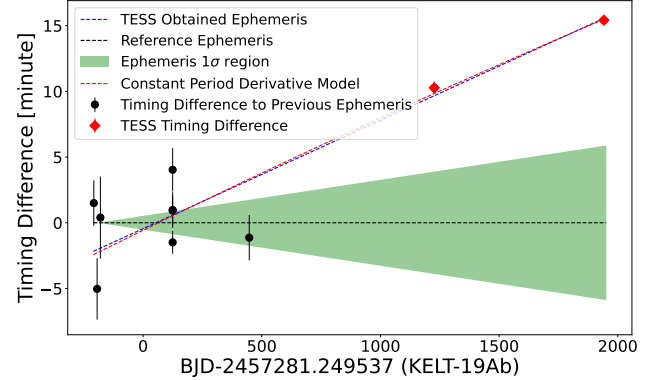


Figure 5. KELT-19Ab timings fitted with a quadratic function. The symbols are similar to Figure 3. The red line shows the quadratic function model.

ing from the underestimation of archival period uncertainties. Period bias caused by a timing shift of 2 minutes would be only $\sim 10^{-5}$ days when the time baseline is 1 year.

We argue that a very significant period difference might be attributed to physical period-changing processes. We find in our sample that the targets with offset SNR larger than 10 all present earlier observation timings. These sources are WASP-161b, XO-3b, and KELT-18b, among which WASP-161b and XO-3b are detected with clues of TTVs in our following work (Yang & Chary 2022; Yang & Wei 2022). The period difference caused by systematic underestimation should be unsigned which is not the case. The tidal dissipation could explain the observational phenomenon.

The tidal torque transfers the energy between the star-planet orbit and the rotation of the star and planet (Goldreich & Soter 1966; Lin et al. 1996; Naoz et al. 2011; Wu & Lithwick 2011; Dawson & Johnson 2018; Rodet et al. 2021). The process could cause the period decay and the apsidal precession (Hut 1981; Ragozzine & Wolf 2009). The induced TTV has been discovered in WASP-12b at \sim a few minutes (Campo et al. 2011; Patra et al. 2017). And TESS provides the most recent evidence for WASP-12b TTV (Turner et al. 2021).

We report WASP-161b, which shows the most significant TESS timing offsets in this sample, presenting a period derivative (P) of $-1.16 \times 10^{-7} \pm 2.25 \times 10^{-8}$ (as details described in Yang & Chary 2022). WASP-161b possibly is undergoing tidal dissipation. We have approved CHEOPS (Benz et al. 2021; Maxted et al. 2021) for two visit observations in 2022 for further investigation. WASP-161b is regarded as a type I target in this work.

The period of XO-3b has been reported differently in previous works (Winn et al. 2008, 2009; Johns-Krull et al. 2008; Wong et al. 2014; Bonomo et al. 2017, and references therein). TESS timing presents an offset of -17.8 ± 1.2 minutes (14.8σ) to the newest archival ephemeris from Bonomo

et al. (2017). The timing generated by our pipeline is consistent within 0.3 minutes to TOI timing. And the uncertainties are similar (~ 0.45 minutes). Yang & Wei (2022) reports the XO-3b as a tidal dissipation candidate by joint analyzing archival timings and TESS timing.

The \dot{P} is $-6.2 \times 10^{-9} \pm 2.9 \times 10^{-10}$ days per orbit per day which relates to a timescale of orbital decay of 1.4 Myr. Applying equilibrium tide (Hut 1981; Leconte et al. 2010), Yang & Wei (2022) obtain a modified tidal quality factor Q'_* as $1.5 \times 10^5 \pm 6 \times 10^3$ if assuming the period decaying is due to the stellar tide. Q'_* is $1.8 \times 10^4 \pm 8 \times 10^2$ under the assumption that period decaying is due to the planetary tide.

The number and properties of the detected dissipating planets would calibrate a series of crucial models in the planet formation theory, e.g., the dissipation as well as circularization timescale, and the possibility of capturing a floating planet or interacting with a stellar companion (Dawson & Johnson 2018).

The apsidal precession could be excited when the tidal torque exists (Ragozzine & Wolf 2009). Distinguishing the difference between tidal dissipation and precession needs to model timings of occultation (Patra et al. 2017; Yee et al. 2020; Turner et al. 2021). XO-3b is also expected to be a candidate presenting precession in previous work (Jordán & Bakos 2008; Antoniciello et al. 2021). We note that the period changing originating from precession and Rømer effect should be unsigned as the same as from systematic underestimation.

The relation between the planet period derivative and host star acceleration rate is well modeled (Bouma et al. 2020). In our sample, KELT-19Ab shows a maximum stellar acceleration at $4 \text{ m s}^{-1} \text{ yr}^{-1}$ originating from binary companion (Siverd et al. 2018b). This acceleration would cause a period derivative of 5.32 ms yr^{-1} , according to the calculation from (Bouma et al. 2020). We generate the TESS timings in both 2019 and 2020. TOI catalog gives the timing at 2020 which is only 0.14 minutes different from our result (as shown in Figure 2 and caption therein). We find timings can be fitted with both a linear and a quadratic function (as shown in Figure 5). The fitting result of the quadratic function indicates a period derivative of $112 \pm 94 \text{ ms yr}^{-1}$. Therefore, we conclude that combining TESS and archival timings do not present a significant TTV dominated by stellar acceleration for KELT-19Ab. We regard the Rømer effect beyond the detection limit in this work.

Further investigation requires long-term measurements with both photometric and spectroscopic instruments. The trend of radial velocity curve if presents indicate stellar companions (Bouma et al. 2020). Modeling timing evolution reveals TTV evidence (Holman et al. 2010; Patra et al. 2017; Yang & Wei 2022). Approved telescope proposals have proved to be effective in analyzing the timing offsets of hot

Jupiter (Ragozzine & Wolf 2009; Patra et al. 2017). Sky surveys, e.g., Kepler, TESS, provide more light curves for timing analysis (Borucki et al. 2011; Ivshina & Winn 2022). Moreover, the sample for relevant analysis can be potentially extended by upcoming time-domain surveys, e.g., Large Synoptic Survey Telescope (LSST; Lund et al. 2015a,b), SiTian (Liu et al. 2021; Yang et al. 2022b).

5. SUMMARY

We discuss the ephemeris of 31 hot Jupiters, of which TOI timings show offsets. We refine the ephemeris of the sample by jointly fitting TESS timings and archival times from previously published papers. The TESS timings are obtained by our self-generated pipeline. The pipeline obtains the light curve from the raw TESS images and fits the light curve with the planet transit model. The result from our pipeline gives consistent results compared to TOI catalog.

Among the sample, TOI timings present a median offset of 17.8 ± 4.9 minutes, equivalent to an SNR of 3.6σ when compared to the previous ephemeris. WASP-161b and XO-3b give the most significant timing offsets. The ephemeris refinement serves the potential follow-up observations for equipment, e.g., CHEOPS, ongoing James Webb Space Telescope, and Ariel Space Telescope. The refined timing reaches a precision within 0.82 minutes in the next 5 years and 1.21 minutes in the next ten years.

WASP-161b, XO-3b, and KELT-18b present timing offsets larger than 10σ . These three targets all have an earlier observed timing than the predictions from the previous ephemeris under a constant period assumption. We find WASP-161b and XO-3b present evidence of period decaying (Yang & Chary 2022; Yang & Wei 2022). Apsidal precession could be an alternative explanation to the TTVs. Interestingly, all four targets (WASP-161, XO-3b, WASP-12b, WASP-4b) reported with observed TTVs, show earlier timing than the prediction in a constant period model. Apsidal precession could not explain this since the timing variation caused by precession should be unsigned. Further observations, e.g., occultation timing monitoring, are helpful for confirmation.

ACKNOWLEDGEMENTS

This work made use of the NASA Exoplanet Archive² (Akeson et al. 2013) and PyAstronomy³ (Czesla et al. 2019). We would like to thank for Ranga-Ram Chary for helpful discussions. Su-Su Shan, Fan Yang, and Ji-Feng Liu acknowledge fundings from the National Key Research and Development Program of China (No.2016YFA0400800), the National Natural Science Foundation of China (NSFC;

² <https://exoplanetarchive.ipac.caltech.edu/index.html>

³ <https://github.com/szczesla/PyAstronomy>

No.11988101), the CSST MilkyWay and Nearby Galaxies Survey on Dust and Extinction Project CMS-CSST-2021-A09 and the Cultivation Project for LAMOST Scientific Payoff and Research Achievement of CAMS-CAS. Hai-Yan Zhang acknowledges NSFC (No.12041301, U1831128). Xing Wei is supported by NSFC (No.11872246, 12041301), and the Beijing Natural Science Foundation (No. 1202015).

APPENDIX

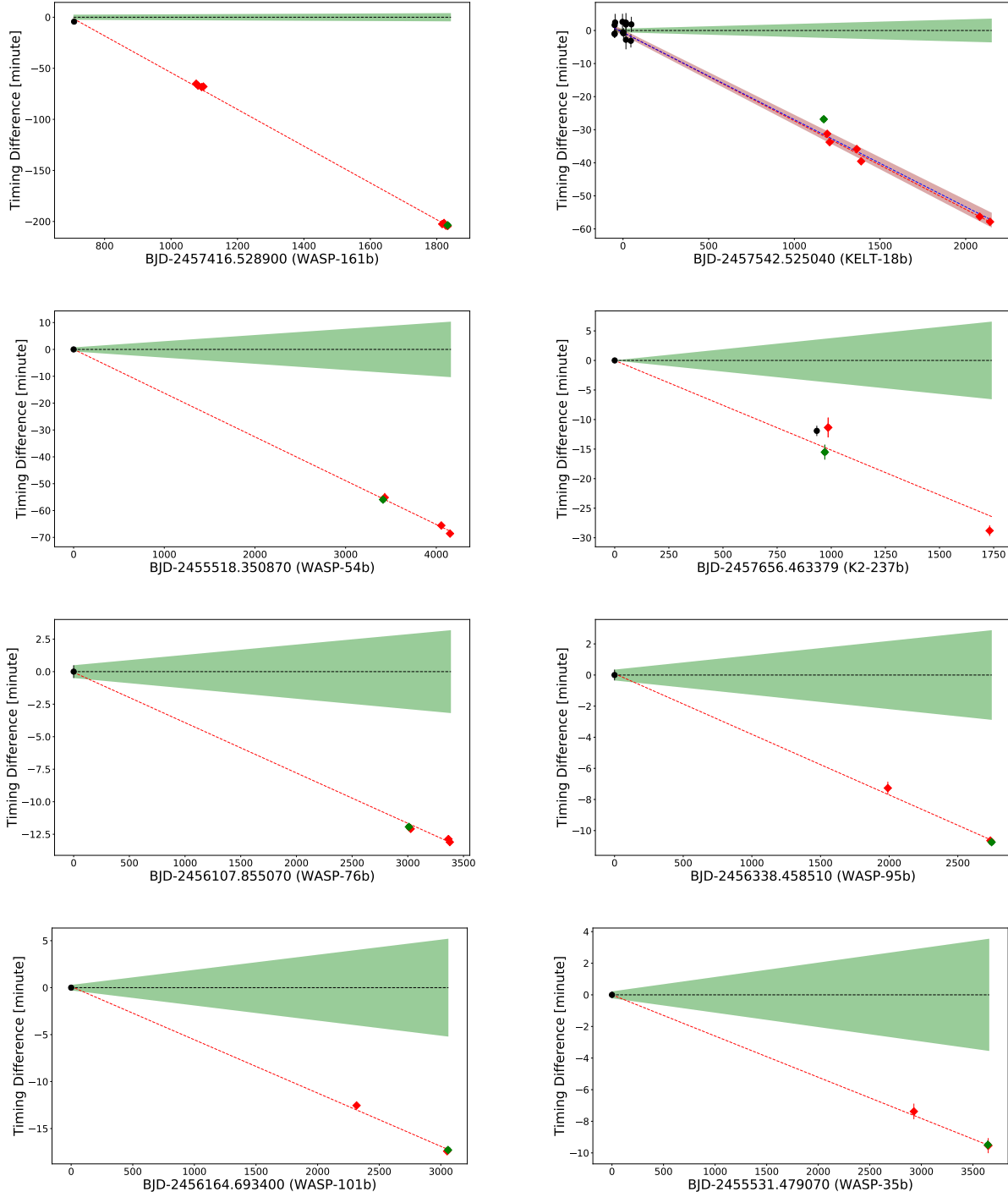
Fig. Set 1. Timing differences of Type I targets of which the timings can be fitted by a linear function. The symbols are the same as Figure 3 while the legend inside the image is dismissed for clarity.

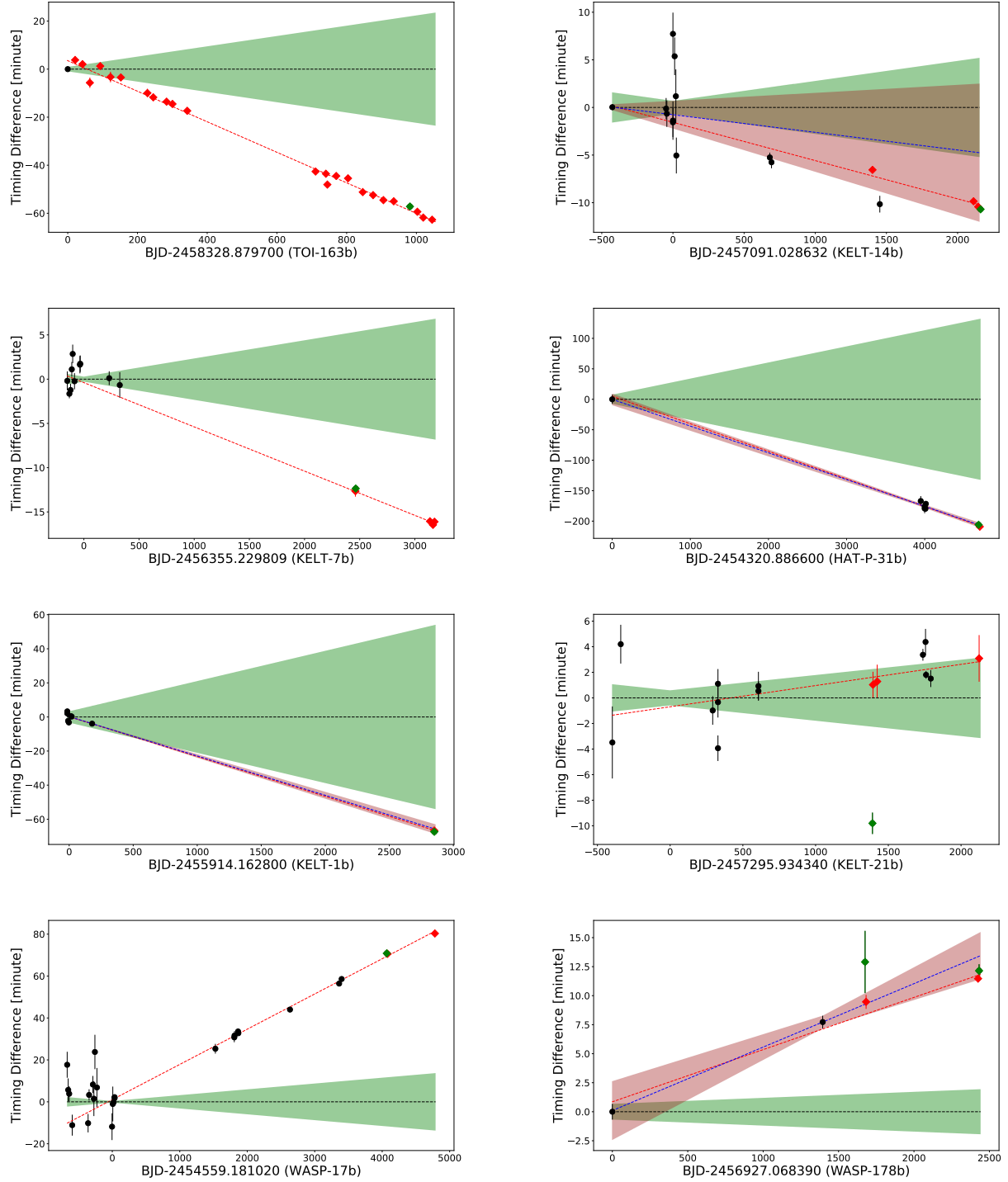
Fig. Set 2. Timing differences of Type II targets of which timings would be modeled by a quadratic function.

Fig. Set 3. Timing differences of Type III targets of which the timings can not be fitted with any linear or quadratic functions. The symbols are the same as Figure 3.

Figure A1-A3 shows the timing differences of 31 targets classified by three types.

Figure A1. Timing differences of Type I targets of which the timings can be fitted by a linear function. The symbols are the same as Figure 3 and the legend inside the image is dismissed for clarity.



**Figure A1.** (Continued)

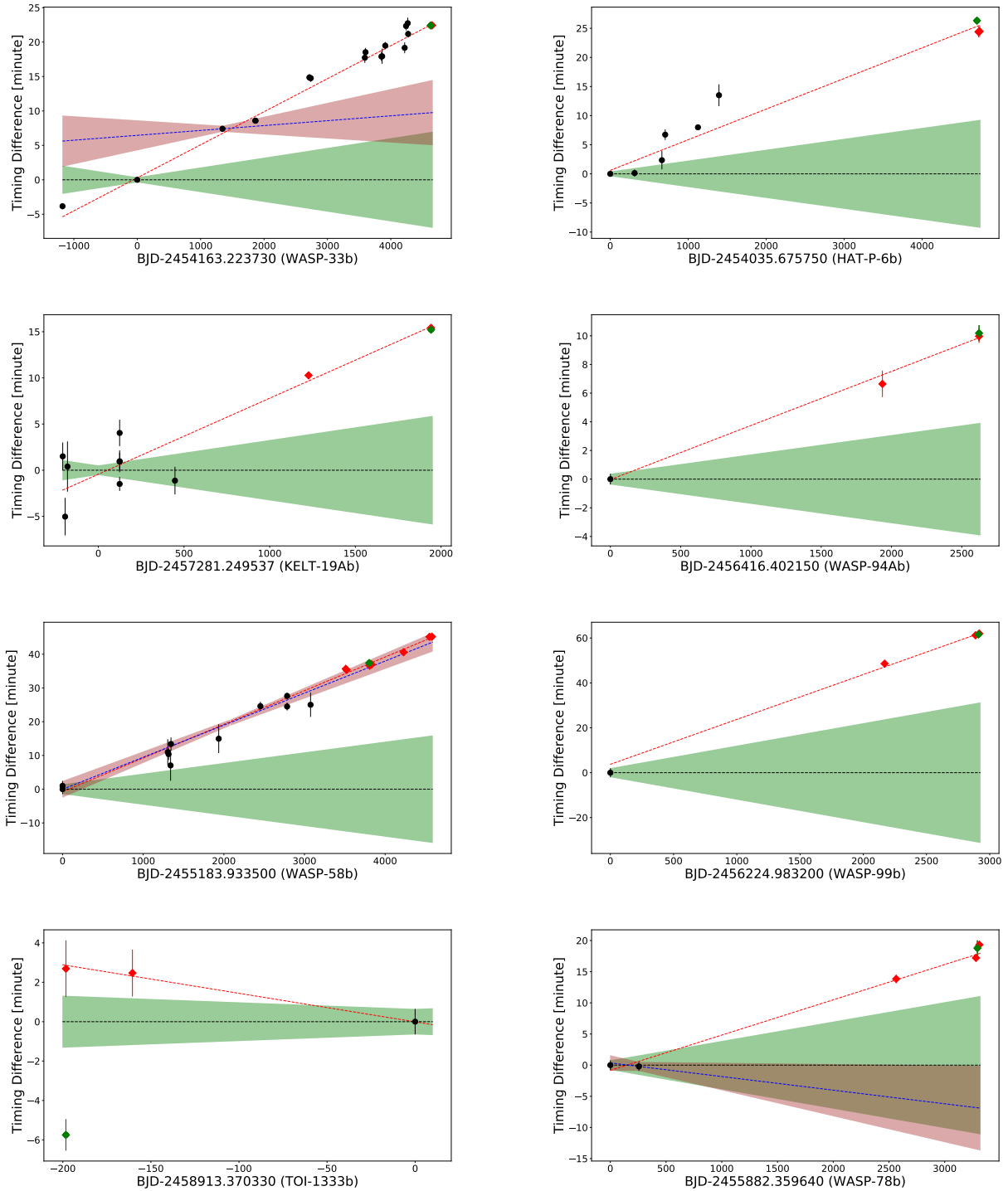


Figure A1. (Continued)

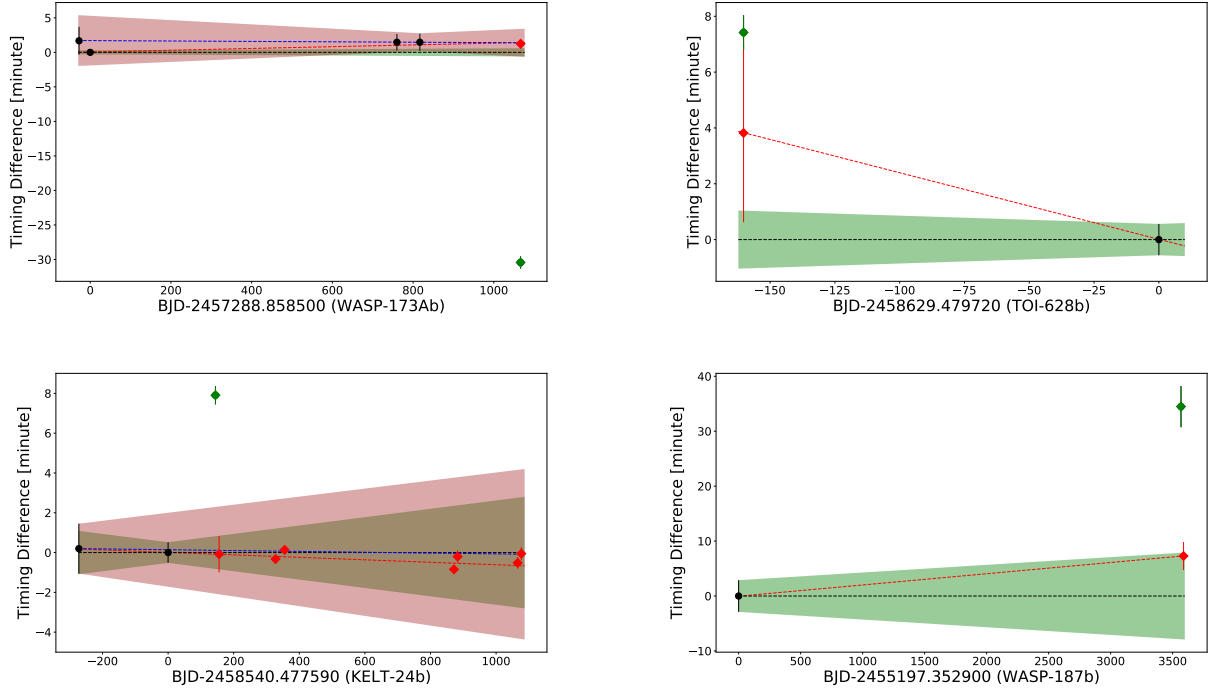
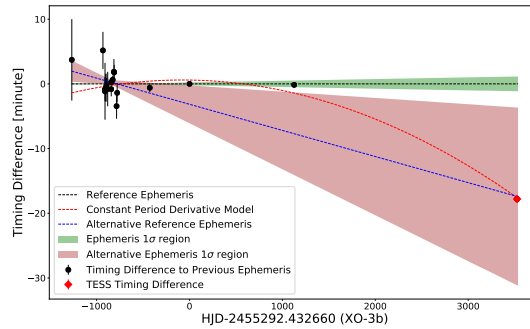
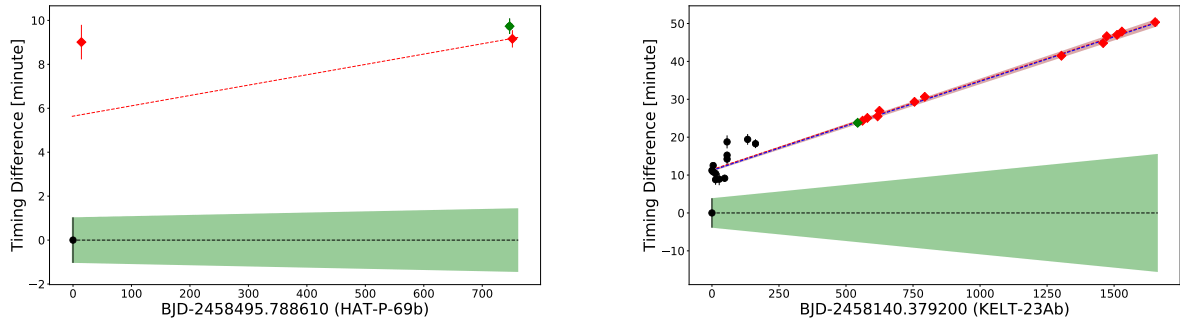
**Figure A1.** (Continued)**Figure A2.** Timing differences of Type II targets of which timings would be modeled by a quadratic function.**Figure A3.** Timing differences of Type III targets of which the timings can not be fitted with any linear or quadratic functions.

Table 2. The single mid-transit times of each target from the literature if available.

Planet ID	Mid-Transit time T BJD_{TDB}	Reference
WASP-161b	2458492.286046±0.00140	Yang & Chary (2022)
	2458497.690811±0.00140	Yang & Chary (2022)
	2458508.501901±0.00140	Yang & Chary (2022)
	2458513.908266±0.00140	Yang & Chary (2022)
	2459232.818367±0.00094	Yang & Chary (2022)
	2459238.225141±0.00094	Yang & Chary (2022)
	2459243.629420±0.00094	Yang & Chary (2022)
	2459249.035140±0.00094	Yang & Chary (2022)
XO-3b	2458819.06428±0.00035	Yang & Wei (2022)
	2458822.25556±0.00034	Yang & Wei (2022)
	2458825.44732±0.00037	Yang & Wei (2022)
	2458831.83008±0.00035	Yang & Wei (2022)
	2458835.02191±0.00034	Yang & Wei (2022)
	2458838.21397±0.00042	Yang & Wei (2022)
	2454864.76684±0.00040	Yang & Wei (2022)
	2454025.3967±0.0038	Yang & Wei (2022)
	2454360.50866±0.00173	Winn et al. (2008)
	2454382.84500±0.00265	Winn et al. (2008)
	2454382.84523±0.00112	Winn et al. (2008)
	2454392.41999±0.00130	Winn et al. (2008)
	2454395.61179±0.00167	Winn et al. (2008)
	2454398.80332±0.00066	Winn et al. (2008)
	2454411.56904±0.00161	Winn et al. (2008)
	2454449.86742±0.00067	Winn et al. (2008)
	2454465.82610±0.00038	Winn et al. (2008)
	2454478.59308±0.00119	Winn et al. (2008)
	2454481.78455±0.00070	Winn et al. (2008)
	2454507.31319±0.00118	Winn et al. (2008)
	2454513.69768±0.00090	Winn et al. (2008)
KELT-18b	2457493.70451 ^{+0.00082} _{-0.00084}	McLeod et al. (2017)
	2457493.7064±0.0011	McLeod et al. (2017)
	2457493.7046 ^{+0.00086} _{-0.00087}	McLeod et al. (2017)
	2457496.5787 ^{+0.0017} _{-0.0018}	McLeod et al. (2017)
	2457539.6551±0.0017	McLeod et al. (2017)
	2457545.3962±0.0011	McLeod et al. (2017)
	2457559.7568±0.0011	McLeod et al. (2017)
	2457559.7572±0.0020	McLeod et al. (2017)
	2457559.7536 ^{+0.0019} _{-0.0020}	McLeod et al. (2017)
	2457588.4709 ^{+0.0014} _{-0.0013}	McLeod et al. (2017)
	2457591.3461 ^{+0.0015} _{-0.0016}	McLeod et al. (2017)
K2-237b	2458589.73380±0.00061	Edwards et al. (2021b)
KELT-14b	2457043.146899±0.000775	Rodriguez et al. (2016)
	2457048.276707±0.000961	Rodriguez et al. (2016)
	2457091.027548±0.001076	Rodriguez et al. (2016)
	2457091.033997±0.001551	Rodriguez et al. (2016)

Continued on next page

Table 2 – *Continued from previous page*

Planet ID	T BJD_{TDB}	Reference
	2457091.027674±0.001400 2457103.002776±0.001377 2457111.550157±0.001956 2457114.965950±0.001308 2457771.62839±0.00035 2457783.59845±0.00044 2458544.57156±0.00061	Rodriguez et al. (2016) Rodriguez et al. (2016) Rodriguez et al. (2016) Rodriguez et al. (2016) Edwards et al. (2021b) Edwards et al. (2021b) Edwards et al. (2021b)
KELT-7b	2456204.817057±0.000741 2456223.959470±0.000358 2456234.898861±0.000486 2456245.839584±0.000579 2456254.045118±0.000730 2456270.451621±0.000637 2456319.678871±0.000683 2456322.413721±0.000648 2456584.950978±0.000544 2456680.667558±0.001007	Bieryla et al. (2015) Bieryla et al. (2015)
HAT-P-31b	2458270.05094±0.00564 2458320.09907±0.00131 2458320.09673±0.00550 2458330.10726±0.00340 2458335.11829±0.00213	Mallonn et al. (2019) Mallonn et al. (2019) Mallonn et al. (2019) Mallonn et al. (2019) Mallonn et al. (2019)
KELT-1b	2455899.5549±0.0010 2455899.55408±0.00044 2455905.63860 ^{+0.00084} _{-0.00082} 2455911.72553±0.00045 2455927.55574 ^{+0.00040} _{-0.00042} 2455933.64320 ^{+0.00041} _{-0.0003}	Siverd et al. (2012) Siverd et al. (2012)
KELT-21b	2456898.527802±0.001956 2456956.337374±0.001053 2457588.567597±0.000775 2457624.696694±0.000799 2457624.695694±0.000833 2457624.693194±0.000694 2457902.879452±0.000775 2457902.879181±0.000521 2459033.67650±0.00032 2459051.74102±0.00071 2459055.35200±0.00021 2459087.86668±0.00046	Johnson et al. (2018) Johnson et al. (2018) Garai et al. (2022) Garai et al. (2022) Garai et al. (2022) Garai et al. (2022)
WASP-17b	2453890.549230±0.004306 2453905.482660±0.003819 2453920.423160±0.0025 2453965.238059±0.003472 2454200.571537±0.003056 2454215.522667±0.001875	Anderson et al. (2010) Anderson et al. (2010)

Continued on next page

Table 2 – *Continued from previous page*

Planet ID	T BJD_{TDB}	Reference
	2454271.557737±0.002847	Anderson et al. (2010)
	2454286.494817±0.005764	Anderson et al. (2010)
	2454301.452058±0.005694	Anderson et al. (2010)
	2454331.323827±0.006458	Anderson et al. (2010)
	2454555.437350±0.004444	Anderson et al. (2010)
	2454566.651190±0.005764	Anderson et al. (2010)
	2454592.801221±0.000382	Anderson et al. (2010)
	2456423.18973±0.00023	Alderson et al. (2022)
	2456426.9246±0.0003	Alderson et al. (2022)
	2457921.1177278±0.000775	Alderson et al. (2022)
	2457958.473652±0.000775	Alderson et al. (2022)
	2456367.15615529±0.001615	Alderson et al. (2022)
	2456086.99426107±0.001615	Alderson et al. (2022)
	2456370.8921914±0.001499	Alderson et al. (2022)
WASP-33b	2452984.82964±0.00030	Turner et al. (2016a)
	2456029.62604±0.0001624	Zhang et al. (2018)
	2456024.74659±0.00014	Zhang et al. (2018)
	2456878.65777±0.00033	Maciejewski et al. (2018)
	2456900.61530±0.00036	Maciejewski et al. (2018)
	2457753.30433±0.00052	Maciejewski et al. (2018)
	2457764.28369±0.00043	Maciejewski et al. (2018)
	2458015.57583±0.00046	Maciejewski et al. (2018)
	2458026.55466±0.00077	Maciejewski et al. (2018)
	2458075.35041±0.00037	Maciejewski et al. (2018)
	2458381.53678±0.00055	Maciejewski et al. (2018)
	2458403.49659±0.00045	Maciejewski et al. (2018)
	2458430.33394±0.00056	Maciejewski et al. (2018)
	2458436.43219±0.00034	Maciejewski et al. (2018)
KELT-23Ab	2458144.898400±0.000463	Johns et al. (2019)
	2458144.897240±0.000440	Johns et al. (2019)
	2458153.917930±0.000590	Johns et al. (2019)
	2458153.916810±0.000949	Johns et al. (2019)
	2458167.448400±0.001100	Johns et al. (2019)
	2458187.745830±0.000637	Johns et al. (2019)
	2458196.770350±0.001100	Johns et al. (2019)
	2458196.771060±0.000625	Johns et al. (2019)
	2458196.773500±0.001192	Johns et al. (2019)
	2458273.452490±0.000984	Johns et al. (2019)
	2458302.769970±0.000810	Johns et al. (2019)
HAT-P-6b	2454347.76763±0.00042	Szabo et al. (2010)
	2454698.3908±0.0011	Szabo et al. (2010)
	2454740.77668±0.00063	Todorov et al. (2012)
	2455160.75292±0.00034	Todorov et al. (2012)
	2455430.4657±0.0013	Todorov et al. (2012)
KELT-19Ab	2457073.723660±0.001042	Siverd et al. (2018a)
	2457087.554255±0.001412	Siverd et al. (2018a)

Continued on next page

Table 2 – *Continued from previous page*

Planet ID	T BJD_{TDB}	Reference
	2457101.393149±0.001887	Siverd et al. (2018a)
	2457405.764653±0.000521	Siverd et al. (2018a)
	2457405.766335±0.000683	Siverd et al. (2018a)
	2457405.768490±0.000995	Siverd et al. (2018a)
	2457405.766362±0.000822	Siverd et al. (2018a)
	2457728.584553±0.001042	Siverd et al. (2018a)
WASP-58b	2455183.9342±0.0010	Mallonn et al. (2019)
	2456488.40790±0.00264	Mallonn et al. (2019)
	2456498.44187±0.00121	Mallonn et al. (2019)
	2456523.52545±0.00316	Mallonn et al. (2019)
	2456528.54704±0.00134	Mallonn et al. (2019)
	2457120.57537±0.00297	Mallonn et al. (2019)
	2457637.35161±0.0008975	Mallonn et al. (2019)
	2457968.48759±0.00068141	Mallonn et al. (2019)
	2457968.48541±0.00082141	Mallonn et al. (2019)
	2458259.48221±0.00249199	Mallonn et al. (2019)
WASP-173Ab	2457261.1266 ^{+0.0013} _{-0.0014}	Labadie-Bartz et al. (2019)
	2458048.74546 ^{+0.00084} _{-0.00078}	Labadie-Bartz et al. (2019)
	2458105.59824 ^{+0.00090} _{-0.00084}	Labadie-Bartz et al. (2019)

REFERENCES

- Agol, E., Cowan, N. B., Knutson, H. A., et al. 2010, ApJ, 721, 1861
 Agol, E., & Fabrycky, D. C. 2018, Transit-Timing and Duration Variations for the Discovery and Characterization of Exoplanets, ed. H. J. Deeg & J. A. Belmonte, 7
 Akeson, R. L., Chen, X., Ciardi, D., et al. 2013, PASP, 125, 989
 Alderson, L., Wakeford, H. R., MacDonald, R. J., et al. 2022, MNRAS, 512, 4185
 Anderson, D. R., Hellier, C., Gillon, M., et al. 2010, ApJ, 709, 159
 Anderson, D. R., Smith, A. M. S., Lanotte, A. A., et al. 2011, MNRAS, 416, 2108
 Andrae, R., Schulze-Hartung, T., & Melchior, P. 2010, arXiv e-prints, arXiv:1012.3754
 Antoniciello, G., Borsato, L., Lacedelli, G., et al. 2021, MNRAS, 505, 1567
 Baluev, R. V., Sokov, E. N., Shaidulin, V. S., et al. 2015, MNRAS, 450, 3101
 Barkaoui, K., Burdanov, A., Hellier, C., et al. 2019, AJ, 157, 43
 Benz, W., Broeg, C., Fortier, A., et al. 2021, Experimental Astronomy, 51, 109
 Berta, Z. K., Charbonneau, D., Désert, J.-M., et al. 2012, ApJ, 747, 35
 Bieryla, A., Collins, K., Beatty, T. G., et al. 2015, AJ, 150, 12
 Bonomo, A. S., Desidera, S., Benatti, S., et al. 2017, A&A, 602, A107
 Borucki, W. J., Koch, D. G., Basri, G., et al. 2011, ApJ, 736, 19
 Bouma, L. G., Winn, J. N., Howard, A. W., et al. 2020, ApJL, 893, L29
 Bouma, L. G., Winn, J. N., Baxter, C., et al. 2019, AJ, 157, 217
 Brown, D. J. A., Triaud, A. H. M. J., Doyle, A. P., et al. 2017, MNRAS, 464, 810
 Campo, C. J., Harrington, J., Hardy, R. A., et al. 2011, ApJ, 727, 125
 Claret, A. 2018, A&A, 618, A20
 Collier Cameron, A., Guenther, E., Smalley, B., et al. 2010, MNRAS, 407, 507
 Czesla, S., Schröter, S., Schneider, C. P., et al. 2019, PyA: Python astronomy-related packages, , ascl:1906.010
 Dawson, R. I., & Johnson, J. A. 2018, ARA&A, 56, 175
 Deming, D., Wilkins, A., McCullough, P., et al. 2013, ApJ, 774, 95
 Eastman, J., Gaudi, B. S., & Agol, E. 2013, PASP, 125, 83
 Edwards, B., Changeat, Q., Yip, K. H., et al. 2021a, MNRAS, 504, 5671
 —. 2021b, MNRAS, 504, 5671
 Enoch, B., Anderson, D. R., Barros, S. C. C., et al. 2011, AJ, 142, 86
 Gaia Collaboration, Brown, A. G. A., Vallenari, A., et al. 2018a, A&A, 616, A1
 —. 2018b, A&A, 616, A1

- Garai, Z., Pribulla, T., Kovács, J., et al. 2022, MNRAS, arXiv:2204.09077
- Goldreich, P., & Soter, S. 1966, Icarus, 5, 375
- Guerrero, N. M., Seager, S., Huang, C. X., et al. 2021, ApJS, 254, 39
- Hébrard, G., Collier Cameron, A., Brown, D. J. A., et al. 2013, A&A, 549, A134
- Hellier, C., Anderson, D. R., Collier Cameron, A., et al. 2014, MNRAS, 440, 1982
- Hellier, C., Anderson, D. R., Bouchy, F., et al. 2019, MNRAS, 482, 1379
- Holman, M. J., Fabrycky, D. C., Ragozzine, D., et al. 2010, Science, 330, 51
- Howard, W. S., Teske, J., Corbett, H., et al. 2021, arXiv e-prints, arXiv:2106.15638
- Huang, C., Wu, Y., & Triaud, A. H. M. J. 2016, ApJ, 825, 98
- Huang, C. X., Vanderburg, A., Pál, A., et al. 2020, Research Notes of the American Astronomical Society, 4, 204
- Hut, P. 1981, A&A, 99, 126
- Ivshina, E. S., & Winn, J. N. 2022, arXiv e-prints, arXiv:2202.03401
- Jenkins, J. M. 2002, ApJ, 575, 493
- Johns, D., Reed, P. A., Rodriguez, J. E., et al. 2019, AJ, 158, 78
- Johns-Krull, C. M., McCullough, P. R., Burke, C. J., et al. 2008, ApJ, 677, 657
- Johnson, M. C., Rodriguez, J. E., Zhou, G., et al. 2018, AJ, 155, 100
- Jordán, A., & Bakos, G. Á. 2008, ApJ, 685, 543
- Kass, R. E., & Raftery, A. E. 1995, Journal of the American Statistical Association, 90, 773
- Kipping, D. M. 2010, MNRAS, 408, 1758
- . 2013, MNRAS, 435, 2152
- Kipping, D. M., Hartman, J., Bakos, G. Á., et al. 2011, AJ, 142, 95
- Kossakowski, D., Espinoza, N., Brahm, R., et al. 2019, MNRAS, 490, 1094
- Kreidberg, L. 2015, PASP, 127, 1161
- Labadie-Bartz, J., Rodriguez, J. E., Stassun, K. G., et al. 2019, ApJS, 240, 13
- Lai, D., Helling, C., & van den Heuvel, E. P. J. 2010, ApJ, 721, 923
- Leconte, J., Chabrier, G., Baraffe, I., & Levrard, B. 2010, A&A, 516, A64
- Lendl, M., Triaud, A. H. M. J., Anderson, D. R., et al. 2014, A&A, 568, A81
- Lin, D. N. C., Bodenheimer, P., & Richardson, D. C. 1996, Nature, 380, 606
- Liu, J., Soria, R., Wu, X.-F., Wu, H., & Shang, Z. 2021, An. Acad. Bras. Ciênc. vol.93 suppl.1, 93, 20200628
- Lund, M. B., Pepper, J., & Stassun, K. G. 2015a, AJ, 149, 16
- . 2015b, AJ, 149, 16
- Maciejewski, G. 2020, AcA, 70, 181
- Maciejewski, G., Fernández, M., Aceituno, F., et al. 2018, AcA, 68, 371
- Makarov, V. V., Beichman, C. A., Catanzarite, J. H., et al. 2009, ApJL, 707, L73
- Mallonn, M., von Essen, C., Herrero, E., et al. 2019, A&A, 622, A81
- Mandel, K., & Agol, E. 2002, ApJ, 580, L171
- Martins, B. L. C., Gomes, R. L., Messias, Y. S., et al. 2020, ApJS, 250, 20
- Maxted, P. F. L., Ehrenreich, D., Wilson, T. G., et al. 2021, MNRAS, arXiv:2111.08828
- Mazeh, T., Nachmani, G., Holczer, T., et al. 2013, ApJS, 208, 16
- McLeod, K. K., Rodriguez, J. E., Oelkers, R. J., et al. 2017, AJ, 153, 263
- Millholland, S., & Laughlin, G. 2018, ApJL, 869, L15
- Naoz, S., Farr, W. M., Lithwick, Y., Rasio, F. A., & Teyssandier, J. 2011, Nature, 473, 187
- Noyes, R. W., Bakos, G. Á., Torres, G., et al. 2008, ApJL, 673, L79
- Patil, A., Huard, D., & Fonnebeck, C. J. 2010, J. Stat. Softw, 1
- Patra, K. C., Winn, J. N., Holman, M. J., et al. 2017, AJ, 154, 4
- Pearson, K. A. 2019, AJ, 158, 243
- Ragozzine, D., & Wolf, A. S. 2009, ApJ, 698, 1778
- Ricker, G. R., Winn, J. N., Vanderspek, R., et al. 2015, Journal of Astronomical Telescopes, Instruments, and Systems, 1, 014003
- Rodet, L., Su, Y., & Lai, D. 2021, ApJ, 913, 104
- Rodriguez, J. E., Colón, K. D., Stassun, K. G., et al. 2016, AJ, 151, 138
- Rodriguez, J. E., Eastman, J. D., Zhou, G., et al. 2019, AJ, 158, 197
- Rodriguez, J. E., Quinn, S. N., Zhou, G., et al. 2021, AJ, 161, 194
- Rodríguez Martínez, R., Gaudi, B. S., Rodriguez, J. E., et al. 2020, AJ, 160, 111
- Schanche, N., Hébrard, G., Collier Cameron, A., et al. 2020, MNRAS, 499, 428
- Schwarzenberg-Czerny, A. 1989, MNRAS, 241, 153
- Sedaghati, E., Boffin, H. M. J., Jeřabková, T., et al. 2016, A&A, 596, A47
- Sing, D. K. 2010, A&A, 510, A21
- Siverd, R. J., Beatty, T. G., Pepper, J., et al. 2012, ApJ, 761, 123
- Siverd, R. J., Collins, K. A., Zhou, G., et al. 2018a, AJ, 155, 35
- . 2018b, AJ, 155, 35
- Smith, A. M. S., Csizmadia, S., Gandolfi, D., et al. 2019, AcA, 69, 135
- Southworth, J., Hinse, T. C., Dominik, M., et al. 2012, MNRAS, 426, 1338
- Szabo, G. M., Haja, O., Szatmary, K., Pal, A., & Kiss, L. L. 2010, Information Bulletin on Variable Stars, 5919, 1
- Thompson, S. E., Coughlin, J. L., Hoffman, K., et al. 2018, ApJS, 235, 38
- Todorov, K. O., Deming, D., Knutson, H. A., et al. 2012, ApJ, 746, 111

- Triaud, A. H. M. J., Neveu-VanMalle, M., Lendl, M., et al. 2017, *MNRAS*, 467, 1714
- Turner, J. D., Ridden-Harper, A., & Jayawardhana, R. 2021, *AJ*, 161, 72
- Turner, J. D., Pearson, K. A., Biddle, L. I., et al. 2016a, *MNRAS*, 459, 789
- Turner, O. D., Anderson, D. R., Collier Cameron, A., et al. 2016b, *PASP*, 128, 064401
- Twicken, J. D., Jenkins, J. M., Seader, S. E., et al. 2016, *AJ*, 152, 158
- von Essen, C., Czesla, S., Wolter, U., et al. 2014, *A&A*, 561, A48
- Wang, X.-Y., Wang, Y.-H., Wang, S., et al. 2021, arXiv e-prints, arXiv:2105.14851
- West, R. G., Hellier, C., Almenara, J. M., et al. 2016, *A&A*, 585, A126
- Winn, J. N., Holman, M. J., Torres, G., et al. 2008, *ApJ*, 683, 1076
- Winn, J. N., Johnson, J. A., Fabrycky, D., et al. 2009, *ApJ*, 700, 302
- Wong, I., Knutson, H. A., Cowan, N. B., et al. 2014, *ApJ*, 794, 134
- Wu, Y., & Lithwick, Y. 2011, *ApJ*, 735, 109
- Yang, F., & Chary, R.-R. 2022, arXiv e-prints, arXiv:2204.12306
- Yang, F., Chary, R.-R., & Liu, J.-F. 2022a, *AJ*, 163, 42
- Yang, F., Shan, S.-S., Guo, R., et al. 2021, *Astrophysics and Space Science*, 366, 83
- Yang, F., & Wei, X. 2022, *PASP*, 134, 024401
- Yang, F., Long, R. J., Shan, S.-S., et al. 2020, *ApJS*, 249, 31
- Yang, F., Long, R. J., Liu, J.-f., et al. 2021, *AJ*, 161, 294
- Yang, F., Zhang, B., Long, R. J., et al. 2021, arXiv e-prints, arXiv:2110.07944
- Yang, F., Wang, W., Wei, X., et al. 2022b, *Research in Astronomy and Astrophysics*, 22, 055005
- Yee, S. W., Winn, J. N., Knutson, H. A., et al. 2020, *ApJL*, 888, L5
- Zhang, M., Knutson, H. A., Kataria, T., et al. 2018, *AJ*, 155, 83
- Zhou, G., Huang, C. X., Bakos, G. Á., et al. 2019, *AJ*, 158, 141